Am J Nucl Med Mol Imaging 2018;8(2):110-118
www.ajnmmi.us /ISSN:2160-8407/ajnmmi0071651

Original Article

Standard OSEM vs. regularized PET image reconstruction: qualitative and quantitative comparison using phantom data and various clinical radiopharmaceuticals

Judit Lantos[1], Erik S Mittra[1], Craig S Levin[1,2,3,4], Andrei Iagaru[1]

Departments of [1]Radiology, [2]Physics, [3]Electrical Engineering, [4]Bioengineering, Stanford University, Stanford 94305, CA, USA

Received December 27, 2017; Accepted February 13, 2018; Epub April 25, 2018; Published April 30, 2018

Abstract: We investigated the block sequential regularized expectation maximization (BSREM) algorithm. ACR phantom measurements with different count statistics and 60 PET/CT research scans from the GE Discovery 600 and 690 scanners were reconstructed using BSREM and the standard-of-care OSEM algorithm. Hot concentration recovery and cold contrast recovery were measured from the phantom data. Two experienced nuclear medicine physicians reviewed the clinical images blindly. Liver SNR liver and SUV_{max} of the smallest lesion detected in each patient were also measured. The relationship between the maximum and mean hot concentration recovery remained monotonic below 1.5 maximum concentration recovery. The mean cold contrast recovery remained stable even for decreasing statistics with a highest absolute difference of 4% in air and 2% in bone for each reconstruction method. The D600 images resulted in an average 30% higher SNR than the D690 data for BSREM; there was no difference in SNR results between the two scanners with OSEM. The small lesion SUV_{max} values on the BSREM images with β of 250, 350 and 450, respectively were on average 80%, 60% and 43% (D690) and 42%, 29%, and 21% (D600) higher than in the case of OSEM. In conclusion, BSREM can outperform OSEM in terms of contrast recovery and organ uniformity over a range of PET tracers, but a task dependent regularization strength parameter (beta) selection may be necessary. To avoid image noise and artifacts, our results suggest that using higher beta values (at least 350) may be appropriate, especially if the data has low count statistics.

Keywords: OSEM, BSREM, PET, image, reconstruction

Introduction

Positron emission tomography (PET) combined with computed tomography (CT) is a widely used functional imaging modality for diagnosis, staging and management of various cancer types [1]. The most often used PET image reconstruction algorithm is the ordered subset expectation maximization (OSEM), which is an iterative statistical algorithm. Because image reconstruction is an ill-conditioned problem, image noise increases with number of iterations. To mitigate image noise, the OSEM algorithm is usually stopped before it has converged; additionally, the images are often post-smoothed using various filters [2]. Alternative approaches try to find the optimal stopping point [3] or use regularization in the iteration cycle [4, 5].

A new PET reconstruction tool (Q.Clear®, GE Healthcare, Waukesha, WI) uses the block sequential regularized expectation maximization (BSREM) algorithm [6], which controls noise at higher iterations by applying a relative difference penalty built into the objective function. This enables one to employ more iterations that is required for convergence and better contrast recovery, while mitigating noise amplification. The penalty term in the objective function can be described as:

$$-\beta R(x) = -\beta \sum_{j=1}^{n_v} \sum_{k \in N_j} w_j w_k \frac{(x_j - x_k)^2}{x_j + x_k + \gamma |x_j - x_k|},$$

Table 1. Distribution of the radiopharmaceuticals and scanners used to acquire data

Pharmaceutical	D600	D690	Σ
^{18}F-FPPRGD$_2$	3	7	10
^{68}Ga-DOTATATE	5	5	10
^{18}F-FSPG	7	3	10
^{18}F-FDG	3	7	10
^{18}F-NaF	4	6	10
^{18}F-NaF & ^{18}F-FDG	5	5	10
Σ	27	33	60

where n_v and N_j denote the number of voxels and the neighbors of voxel j, w_j and w_k are local penalty weights, and γ controls the level of edge-preservation.

Different groups have already investigated the relation between standard OSEM and BSREM [7-13] but these studies were performed using only 2-deoxy-2-[fluorine-18]fluoro-D-glucose (FDG). More specialized radiopharmaceuticals (^{90}Y spheres and ^{13}N-ammonia NH_3) were also evaluated in 2 publications [14, 15]. In this study, we compare this algorithm using various radiopharmaceuticals (^{18}F FB-PEG$_3$-E[c(RGDyK)]$_2$ or ^{18}F-FPPRGD$_2$; ^{68}Ga-DOTA-Octreotate or ^{68}Ga-DOTA-TATE; (4S)-4-(3-[(^{18})F] fluoropropyl)-l-glutamate or ^{18}F-FSPG; ^{18}F-FDG; ^{18}F-NaF; combined ^{18}F-NaF and ^{18}F-FDG) using the GE Discovery 600 (without time-of-flight) and GE Discovery 690 (with time-of-flight) PET/CT scanners. Our preliminary results [16, 17] showed that the regularization strength parameter (β) strongly affects the SNR of the images, which can impact the clinical application of the algorithm [18]. This study asks whether it is possible to find a β parameter for non-TOF images that maximizes contrast recovery, but still produces a clinically acceptable noise level, which may be scanner and tracer dependent.

Materials and methods

Phantom study

The ACR phantom [19] was scanned on the GE Discovery 600 (D600) and 690 (D690) PET/CT scanners using a standard 10 min long acquisition protocol. The faceplate of the cylindrical phantom has four fillable cylinders (8, 12, 16 and 25 mm in diameter) and three cold cylinders (filled with air or bone equivalent material). The lower portion with the cold rods arranged in a pie-shaped pattern was not used in the data analysis. The phantom was filled with a background activity concentration of 6.44 and 6.48 kBq/ml and a hot cylinder concentration of 14.04 and 11.97 kBq/ml in the D600 and D690 measurements, respectively.

The data were truncated to create different measurement statistics between 5 and 100% of the total counts (1.79e8 and 1.37e8, respectively, for the D600 and D690) resulting in measurement times between 20 s and 10 min. The 11 data sets were reconstructed using:

(1) The standard-of-care OSEM algorithm available on the scanners with 2 iterations and 32 subsets for D600 and 2 iterations and 24 subsets for D690 (as recommended by the manufacturer), in both cases using the standard post-filters: an in plane Gaussian filter with 6.4 mm FWHM and an axial triangle filter with the weights of [1 4 1].

(2) The BSREM algorithm with 25 iterations and different regularization strength parameters (β values between 250 and 450) without any post filter applied.

Signal-to-noise ratio (SNR) was measured in the uniform region (middle section) of the phantom and was calculated as the ratio of the pixel-wise mean and standard deviation of the cylindrical region of interest (ROI). The relative SNR difference between the scanners for a given reconstruction method was defined as:

$$\triangle SNR = 1 - \frac{SNR(\text{D690})}{SNR(\text{D600})}.$$

Mean and maximum hot concentration recovery were defined as the ratio between the mean or maximum concentration measured in the hot cylinders (in ROIs with the same diameter as the cylinders) and the actual activity concentration value (from the dose calibrator). To calculate cold contrast recovery the mean concentration values were measured in cylindrical ROIs (same diameter as the cylinders) and were compared to the mean of the uniform region (same as in the SNR calculation). We used the Wilcoxon signed-rank test for statistical comparison.

Patient study

A total of 60 datasets from clinical research PET/CT scans using various radiopharmaceuti-

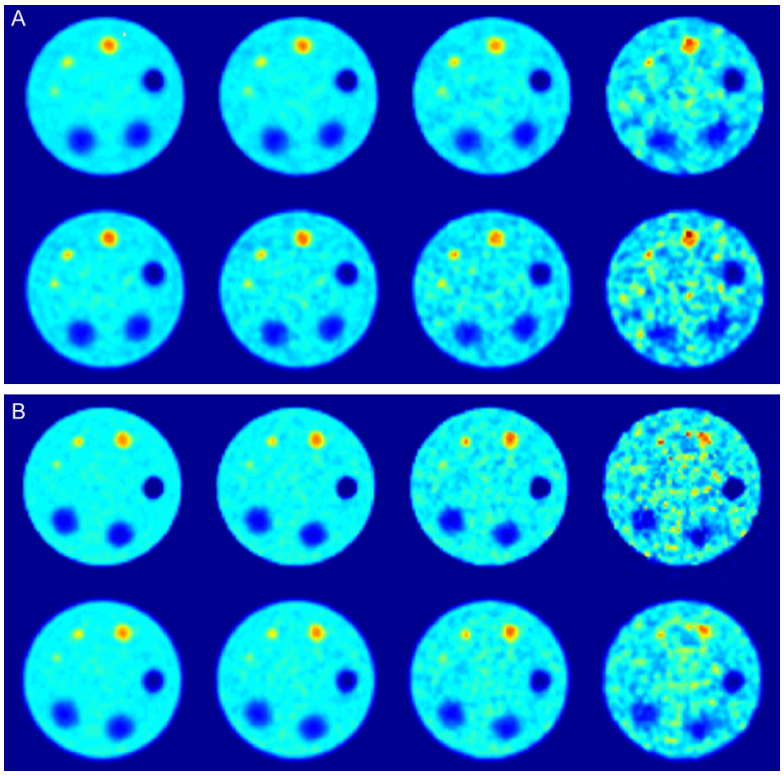

Figure 1. ACR phantom from left to right with 100%, 50%, 20% and 5% of the total counts, respectively; A: D690 top row OSEM, bottom row BSREM β=350; B: D600 top row OSEM, bottom row BSREM β=350.

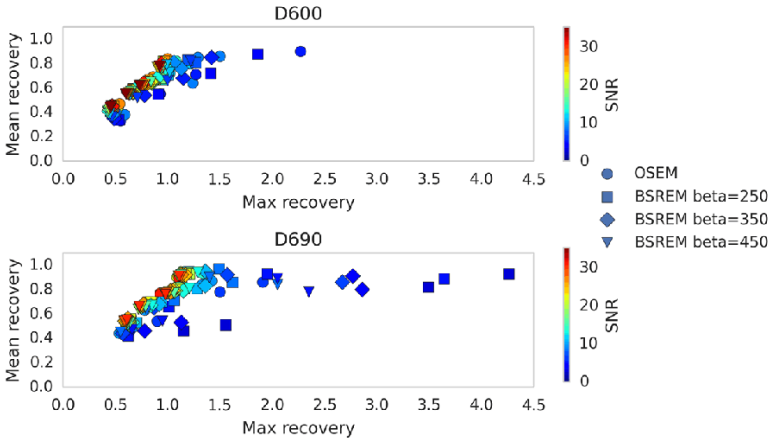

Figure 2. Mean vs. maximum hot concentration recovery for the hot cylinders of the ACR phantom (top: D600, bottom: D690). The different marker shapes depict the 4 reconstruction methods; the marker color represents the SNR value measured in the uniform region of the phantom.

cals were retrospectively reconstructed from the archived sinogram data. The studies involved 31 male and 29 female patients with age between 31-79 (median 57) and Body Mass Index (BMI) between 17.4 and 38.0 (median 26.1). The local institutional review board approved this retrospective study and the requirement to obtain informed consent was waived. For each data set, 3 images were reconstructed using BSREM (with β values of 250, 350 and 450) and compared to standard OSEM reconstruction with reconstruction parameters the same as in the phantom study. The vendor suggested β value of 350, we added lower and higher values in this evaluation. **Table 1** shows the number of patients for each scanner and pharmaceutical type. Each of the 4 reconstructed images/scan were reviewed in random order by 2 nuclear medicine physicians (AI, 11 years of experience interpreting PET; EM, 9 years of experience interpreting PET) using a GE Advantage Workstation version 4.6 workstation and scored 1-5 for visual quality (1 poor, 5 excellent image quality). The readers were blinded to the patients' medical history and characteristics of the image reconstruction. Signal-to-noise ratio i n the liver and maximum standardized uptake values (SUV_{max}) of the smallest lesion detected in each patient were also measured for comparison.

Cohen's kappa test was calculated to evaluate inter-observer agreement of the visual scores. Multivariate regression was performed to analyze the relation of the SUV values, organ homogeneity, and scanner and pharmaceutical type. The relative SUV_{max} measurements were defined as the ratio of the BSREM and OSEM SUV_{max} values for a given lesion. The R 3.1.1 software (R-Project) was

Table 2. Mean cold contrast recovery percentage* averaged over all count statistics for BSREM (β) and OSEM

Reconstruction method	D600		D690	
	Air	Bone	Air	Bone
BSREM (250)	35 ± 1	3 ± 0.6	29 ± 0.4	0.2 ± 0.3
BSREM (350)	37 ± 1	5 ± 0.4	31 ± 0.4	0.4 ± 0.4
BSREM (450)	39 ± 1	8 ± 0.2	32 ± 0.3	0.9 ± 0.4
OSEM	37 ± 1	11 ± 0.2	38 ± 0.5	1.4 ± 0.4

*: Data are given as mean ± standard deviation (%).

used to perform all statistical analyses in this study.

Results

Phantom study

Figure 1 shows the sum of seven slices of the ACR phantom reconstructed from data sets with different statistics. The BSREM image SNR values ranged between 3.95-35.3 (D600) and 2.71-30.7 (D690) while the OSEM images had SNR of 5.51-26.9 (D600) and 6.33-31.0 (D690). When compared at matched count statistics the BSREM images had a 0 to 10% higher relative SNR values for D600 compared to D690 while in the case of OSEM this relative difference was from -33 to -40%.

Figure 2 depicts the relationship between the mean and maximum hot concentration recovery for the four different reconstruction methods for all hot rods and statistics. While the maximum concentration recovery remains under about 1.5 the relation remains monotonic. Above this limit the mean recovery plateaus even when the maximum recovery increases due to image noise. The data points on the far right tend to associate with BSREM with low β and have SNR below 10.

The mean cold contrast recovery remained stable through the decreasing statistics with a highest absolute difference of 4% in air and 2% in bone between the extreme points of each method. **Table 2** shows the average values for the two scanners and four methods. The recovery was significantly higher ($P < 0.01$) for both materials for the D690 and for air for the D600. Interestingly the bone values improved tenfold for BSREM on the D690 images compared to the D600 data.

Clinical study

Figure 3 depicts the liver SNR and smallest lesion SUV_{max} values measured on the patient images. The D600 images resulted in an average 30% higher SNR than the D690 data for BSREM while there was no difference between the scanners with OSEM. The small lesion SUV_{max} values on the BSREM images were in average 80%, 60% and 43% (D690) and 42%, 29%, 21% (D600) higher than in the case of OSEM with β of 250, 350 and 450, respectively. The lesion SUV values were compared using the Wilcoxon signed-rank test adjusted for multiple comparisons; all three BSREM reconstructions resulted in significantly higher values ($P < 0.001$). In the case of 3 patients some small lesions were only identified on BSREM reconstructions. A representative example in the brain confirmed in a follow-up MRI study is shown in **Figure 5**.

To measure the inter-observer agreement of visual quality scores Cohen's kappa was calculated for each OSEM-BSREM pair. Since the agreement was poor (1-5 scale: $\kappa < 0.15$) the observers were not pooled in the analysis. **Table 3** shows the mean visual scores for each observer, reconstruction method and scanner. The scores were significantly higher ($P < 0.02$) for all beta values for the first reader but not for the second reader (after adjusting for multiple comparisons). **Figure 4** shows the relative number of cases when a given method for a given radiopharmaceutical received the highest score out of the 4 images presented to the readers. For a certain patient, often multiple images received the same score hence the ratios do not sum to 1.

To reveal the contribution of the different radiopharmaceuticals on the visual score and the relative small lesion SUV_{max} values (compared to OSEM) we performed a multivariate regression adjusted for reconstruction algorithm, scanner type, reader, liver SNR, and BMI. **Table 4** summarizes the regression coefficients. The visual score coefficients reflected the opposing scoring behaviors of the two readers and showed a significant increase ($P < 0.03$) only for NaF images. The reconstruction method coefficients for the relative SUV_{max} (compared

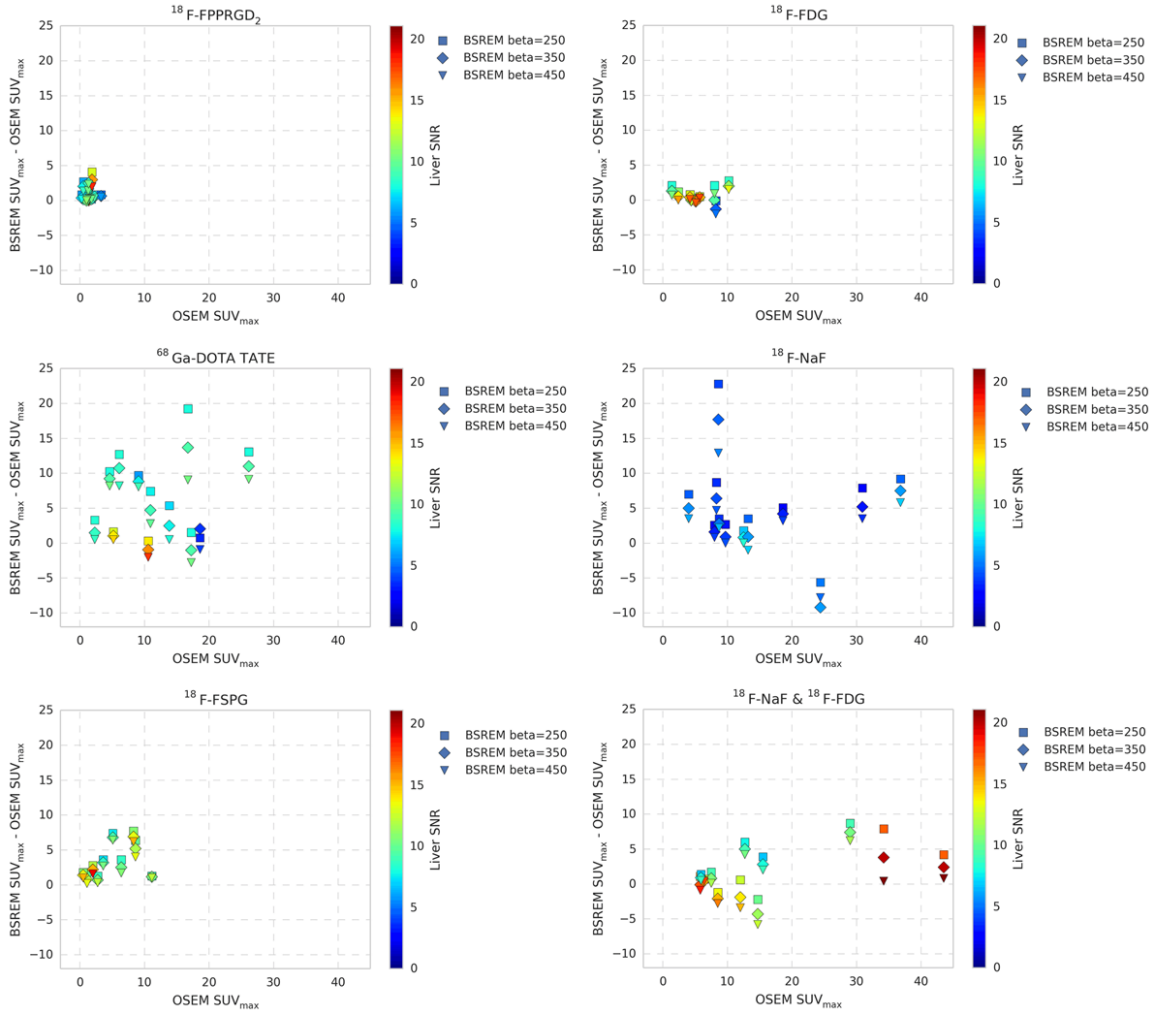

Figure 3. Small lesion SUV_{max} difference between BSREM and OSEM as a function of the OSEM SUV_{max} value in the 60 patient studies using various radiopharmaceuticals. The different marker shapes depict the 3 BSREM β values; the marker color represents the SNR value measured in the liver.

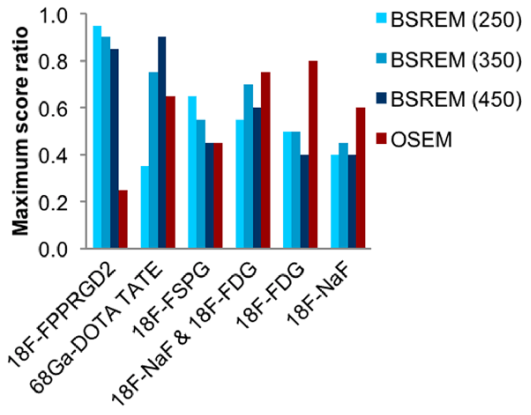

Figure 4. Relative number of cases when a given method for a given radiopharmaceutical received the highest score out of the 4 images presented to the readers.

to OSEM) were significantly higher than 1 ($P < 0.005$) for all three β values, Furthermore, all pharmaceuticals except for the combined NaF and FDG administration contribute to significantly higher ($P < 0.01$) ratios than that for FDG.

Discussion

Here we compared BSREM and OSEM in terms of contrast recovery, SNR, lesion detectability, and organ homogeneity for non-TOF image reconstruction protocols with various radiopharmaceuticals. While other studies focused on FDG and TOF reconstructions, non-TOF scanners still represent a large proportion of the clinical instrumentation [20] and new trac-

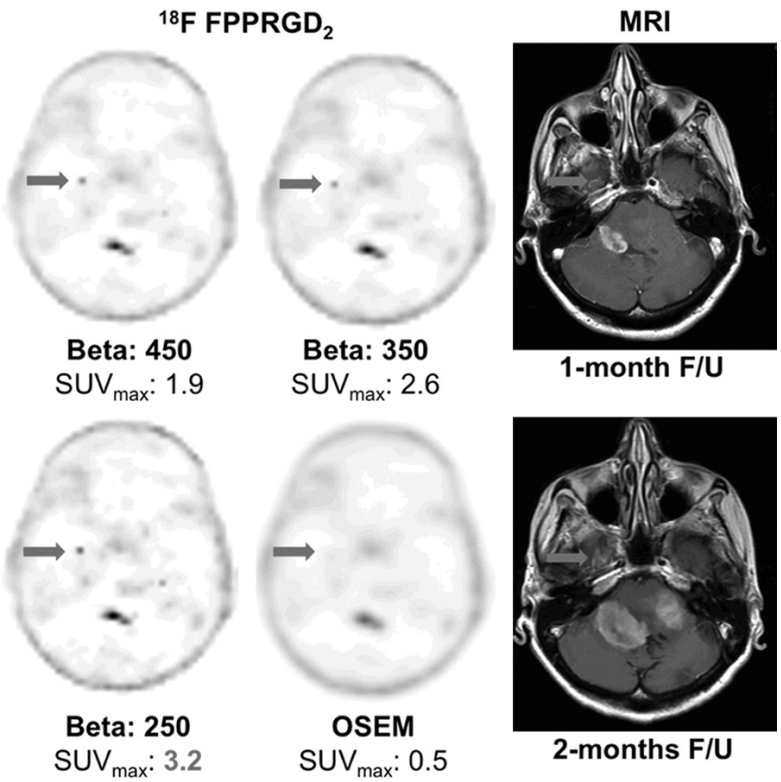

Figure 5. Arrow indicates focal ^{18}F FPPRGD$_2$ uptake visualized on the 3 BSREM reconstructions that is not seen on the OSEM image in a 34-year-old woman with recurrent GBM. Brain MRI follow-up done 1 and 2 months later confirm a growing contrast enhancing lesion in this location.

ers with different biodistribution than FDG are being introduced to research and clinical practice [21, 22].

SUV_{max} is a frequently used metric to describe lesion aggressiveness due to its reproducibility [23]. Ideally, SUV_{max} is proportional to SUV_{mean} hence accurately represents the whole lesion. **Figure 2** suggests that the relation between SUV_{max} and SUV_{mean} are not necessarily monotonic (when SNR and β are too low) which can result in misclassification of image noise, hence using SUV_{peak} is advisable [24].

BSREM gave significantly better cold contrast values than OSEM in both materials for the D690 and for air for the D600 (see **Figure 1** and **Table 2**). Further investigation of the significant relative difference between the bone cold contrast recovery of the scanners showed that while the values decrease for the D690 up to about 10 iterations, the decrease is much lower for the D600 and becomes negligible above 5 iterations. This may be due to the higher spatial resolution of the D690 scanner.

The visual scores showed opposite trends of beta value preference for the two readers (see **Table 3**). This perhaps mainly stems from the difference in image noise tolerance between the two physicians, a "real" variation that occurs in clinical image interpretation. While low beta images are generally richer in details they often contain more uncorrelated random noise than OSEM or BSREM with high beta (see **Figure 5**). When selecting the regularization strength coefficient for a specific protocol (and scanner) the expected count statistics and the desired organ homogeneity level should be considered.

In three patients, we observed that the BSREM algorithm enabled visualization of lesions not seen with OSEM, at least one of which was confirmed with enhancement seen on a follow up MRI. Tools such as Q.Clear® will make very important to have PET tracers specific for particular diseases because small FDG-avid lesions may be non-specific. Finding small lesions that can be anything is not as good as finding small lesions that are cancer; hence our use of targeted radiopharmaceuticals such as ^{18}F-FPPRGD$_2$ [25], ^{68}Ga-DOTATATE [26], and ^{18}F-FSPG [27]. To determine how best to interpret and use these new findings and how it affects clinical management will be a subject of future study. **Figure 4** illustrates how in the case of ^{18}F-FPPRGD$_2$ smaller lesions (confirmed on follow-up imaging to be true positive) were not seen using OSEM, but were conspicuous using BSREM. This may have major implications for patient case, such as selecting the appropriate treatment or assessment of response to therapy.

Our study had four main limitations: the relatively small sample size (given the four pharmaceuticals used), the small number of nuclear

Table 3. Readers' visual scores for image quality*

		Scanner	BSREM (β)			OSEM
			(250)	(350)	(450)	
Visual score	Reader I	D600	4.37 ± .56	4.19 ± .56	4.00 ± .68	3.81 ± .79
		D690	3.85 ± 1.1	3.97 ± .98	3.94 ± .90	3.55 ± .83
		Pooled	4.08 ± .94	4.07 ± .82	3.97 ± .80	3.67 ± .82
	Reader II	D600	3.33 ± .55	3.59 ± .57	3.52 ± .51	3.78 ± .51
		D690	3.06 ± .83	3.39 ± .75	3.48 ± .62	3.67 ± .54
		Pooled	3.18 ± .72	3.48 ± .68	3.50 ± .57	3.72 ± .52

*: Data are given as mean on scale from 1 to 5 ± standard deviation.

Table 4. Linear regression analysis of visual scores‡ and smallest lesion relative SUV_{max} ‡‡

	Visual score		Relative SUV_{max}	
	Estimate	Pr (>|t|)	Estimate	Pr (>|t|)
Intercept	3.6	0.00***	0.58	7.0E-02
BSREM β=250	-0.52	9.6E-05***	0.63	8.9E-10***
BSREM β=350	-0.30	2.7E-02*	0.45	1.5E-05***
BSREM β=450	-0.34	1.4E-02*	0.30	4.4E-03**
BSREM β=250 * Reader1	0.95	5.1E-07***	-	-
BSREM β=350 * Reader1	0.63	7.4E-04***	-	-
BSREM β=450 * Reader1	0.52	5.8E-03**	-	-
^{68}Ga-DOTA TATE	0.01	9.3E-01	0.60	7.0E-05***
^{18}F-FSPG	0.16	2.1E-01	0.65	7.7E-06***
^{18}F-NaF & ^{18}F-FDG	-0.02	8.5E-01	0.15	2.9E-01
^{18}F-FPPRGD$_2$	0.20	1.0E-01	0.46	7.1E-04***
^{18}F-NaF	0.35	2.8E-02*	0.46	9.2E-03**
SUV_{max} (OSEM)	-	-	-0.01	1.4E-03**

‡Model: reconstruction method (categorical, reference: OSEM), reader (categorical: 0/1), radiopharmaceutical (categorical, reference: ^{18}F- FDG), liver SNR (continuous, no unit), relative liver SNR compared to OSEM (continuous, no unit) also adjusted for scanner type (categorical: 0/1), and BMI (continuous, in kg/m^2); ‡‡Model: reconstruction method (categorical, reference: OSEM), radiopharmaceutical (categorical, reference: ^{18}F-FDG), liver SNR (continuous, no unit), small lesion SUV_{max} using OSEM (continuous, no unit), also adjusted for scanner type (categorical: 0/1), and BMI (continuous, in kg/m^2); *Significance codes: 0 '***' 0.001 '**' 0.01 '*' 0.05.

medicine physicians grading the images, the too general "visual quality" criteria for image scoring, and only SUV_{max} values measured for the small lesions. In this *preliminary* study, we were interested in the effect of the different tracers and scanners to see if further, more detailed investigation is necessary to determine optimal parameter protocol selection. Our results suggest that while decreasing beta increases concentration recovery, in clinical practice a higher beta value - between 350 and 450 - is more suitable for all the studied pharmaceuticals. This is in agreement with what others reported for FDG [7, 11].

Conclusion

BSREM can outperform OSEM in terms of contrast recovery and organ uniformity over a range of PET tracers, but a task dependent regularization strength parameter (beta) selection may be necessary. To avoid image noise and artifacts, our results suggest that using higher beta values (at least 350) may be appropriate, especially if the data has low count statistics.

Acknowledgements

The authors would like to thank Shawna Kinsella and Vinh Nguyen for their help with phantom data acquisitions and Stephen G. Ross at GE Healthcare for his valuable comments and his help with image reconstruction.

Disclosure of conflict of interest

None.

Address correspondence to: Dr. Andrei Iagaru, Division of Nuclear Medicine and Molecular Imaging, Department of Radiology, Stanford University, 300 Pasteur Drive, H2200, Stanford 94305-5281, CA, USA. Tel: 650-725-4711; Fax: 650-498-5047; E-mail: aiagaru@stanford.edu

References

[1] Gerd M and Joel SK. Positron emission tomography. Phys Med Biol 2006; 51: R117.

[2] Tong S, Alessio AM and Kinahan PE. Image reconstruction for PET/CT scanners: past achievements and future challenges. Imaging Med 2010; 2: 529-545.

[3] Gaitanis A, Kontaxakis G, Spyrou G, Panayiotakis G and Tzanakos G. PET image reconstruction: a stopping rule for the MLEM algorithm based on properties of the updating coeffi-

cients. Comput Med Imaging Graph 2010; 34: 131-141.
[4] Tsoumpas C, Polycarpou I, Thielemans K, Buerger C, King AP, Schaeffter T and Marsden PK. The effect of regularization in motion compensated PET image reconstruction: a realistic numerical 4D simulation study. Phys Med Biol 2013; 58: 1759.
[5] Wang G and Qi J. Penalized likelihood PET image reconstruction using patch-based edge-preserving regularization. IEEE Trans Med Imaging 2012; 31: 2194-2204.
[6] Ahn S, Fessler JA. Globally convergent image reconstruction for emission tomography using relaxed ordered subsets algorithms. IEEE Trans Med Imaging 2003; 22: 613-626.
[7] Teoh EJ, McGowan DR, Macpherson RE, Bradley KM and Gleeson FV. Phantom and clinical evaluation of the Bayesian penalized likelihood reconstruction algorithm Q.Clear on an LYSO PET/CT system. J Nucl Med 2015; 56: 1447-1452.
[8] Sangtae A, Steven GR, Evren A, Jun M, Xiao J, Lishui C, Scott DW and Ravindra MM. Quantitative comparison of OSEM and penalized likelihood image reconstruction using relative difference penalties for clinical PET. Phys Med Biol 2015; 60: 5733.
[9] Parvizi N, Franklin JM, McGowan DR, Teoh EJ, Bradley KM and Gleeson FV. Does a novel penalized likelihood reconstruction of ^{18}F-FDG PET-CT improve signal-to-background in colorectal liver metastases? Eur J Radiology 2015; 84: 1873-1878.
[10] Teoh EJ, McGowan DR, Bradley KM, Belcher E, Black E and Gleeson FV. Novel penalised likelihood reconstruction of PET in the assessment of histologically verified small pulmonary nodules. Eur Radiology 2016; 26: 576-584.
[11] Sah BR, Stolzmann P, Delso G, Wollenweber SD, Hüllner M, Hakami YA, Queiroz MA, Barbosa FG, von Schulthess GK, Pietsch C, Veit-Haibach P. Clinical evaluation of a block sequential regularized expectation maximization reconstruction algorithm in 18F-FDG PET/CT studies. Nucl Med Commun 2017; 38: 57-66.
[12] Howard BA, Morgan R, Thorpe MP, Turkington TG, Oldan J, James OG and Borges-Neto S. Comparison of Bayesian penalized likelihood reconstruction versus OS-EM for characterization of small pulmonary nodules in oncologic PET/CT. Ann Nucl Med 2017; 31: 623-628.
[13] Vallot D, Caselles O, Chaltiel L, Fernandez A, Gabiache E, Dierickx L, Zerdoud S, Bauriaud M and Courbon F. A clinical evaluation of the impact of the Bayesian penalized likelihood reconstruction algorithm on PET FDG metrics. Nucl Med Commun 2017; 38: 979-984.
[14] Rowley LM, Bradley KM, Boardman P, Hallam A and McGowan DR. Optimization of image reconstruction for 90Y selective internal radiotherapy on a lutetium yttrium orthosilicate PET/CT system using a Bayesian penalized likelihood reconstruction algorithm. J Nucl Med 2017; 58: 658-664.
[15] O'Doherty J, McGowan DR, Abreu C and Barrington S. Effect of Bayesian-penalized likelihood reconstruction on [^{13}N]-NH_3 rest perfusion quantification. J Nucl Cardiol 2017; 24: 282-290.
[16] Lantos J, Iagaru A and Levin C. Standard OSEM vs. Q.Clear® PET image reconstruction: an analysis of phantom data. J Nucl Med 2015; 56: 264.
[17] Lantos J, Mittra E, Levin C and Iagaru A. Standard OSEM vs. regularized PET image reconstruction: qualitative and semi-quantitative comparison. J Nucl Med 2015; 56: 1805.
[18] Morey AM and Kadrmas DJ. Effect of varying number of OSEM Subsets on PET lesion detectability. J Nucl Med Technol 2013; 41: 268-273.
[19] Scheuermann JS, Reddin JS, Opanowski A, Kinahan PE, Siegel BA, Shankar LK and Karp JS. Qualification of NCI-designated cancer centers for quantitative PET/CT imaging in clinical trials. J Nucl Med 2017; 58: 1065-1071.
[20] Sunderland JJ and Christian PE. Quantitative PET/CT scanner performance characterization based upon the society of nuclear medicine and molecular imaging clinical trials network oncology clinical simulator phantom. J Nucl Med 2015; 56: 145-152.
[21] Lopci E, Nanni C, Castellucci P, Montini GC, Allegri V, Rubello D, Chierichetti F, Ambrosini V and Fanti S. Imaging with non-FDG PET tracers: outlook for current clinical applications. Insights Imaging 2010; 1: 373-385.
[22] Schwaiger M and Wester HJ. How many PET tracers do we need? J Nucl Med 2011; 52 Suppl 2: 36S-41S.
[23] Kinahan PE and Fletcher JW. PET/CT standardized uptake values (SUVs) in clinical practice and assessing response to therapy. Semin Ultrasound CT MR 2010; 31: 496-505.
[24] Vanderhoek M, Perlman SB and Jeraj R. Impact of the definition of peak standardized uptake value on quantification of treatment response. J Nucl Med 2012; 53: 4-11.
[25] Minamimoto R, Jamali M, Barkhodari A, Mosci C, Mittra E, Shen B, Chin F, Gambhir SS and Iagaru A. Biodistribution of the ^{18}F-FPPRGD2 PET radiopharmaceutical in cancer patients: an atlas of SUV measurements. Eur J Nucl Med Mol Imaging 2015; 42: 1850-1858.
[26] Moradi F, Jamali M, Barkhodari A, Schneider B, Chin F, Quon A, Mittra ES and Iagaru A. Spec-

trum of ^{68}Ga-DOTA TATE uptake in patients with neuroendocrine tumors. Clin Nucl Med 2016; 41: e281-e287.

[27] Mittra ES, Koglin N, Mosci C, Kumar M, Hoehne A, Keu KV, Iagaru AH, Mueller A, Berndt M, Bullich S, Friebe M, Schmitt-Willich H, Gekeler V, Fels LM, Bacher-Stier C, Moon DH, Chin FT, Stephens AW, Dinkelborg LM and Gambhir SS. Pilot preclinical and clinical evaluation of (4S)-4-(3-[^{18}F]Fluoropropyl)-L-glutamate (^{18}F-FSPG) for PET/CT imaging of intracranial malignancies. PLoS One 2016; 11: e0148628.